Electrostatic charging and deflection of droplets for drop-on-demand 3D printing within confinements

J. Plog, Y. Jiang, Y. Pan*, A.L. Yarin*

Department of Mechanical and Industrial Engineering, University of Illinois at Chicago, 842 W. Taylor St., Chicago, IL, 60607-7022, USA

ARTICLE INFO

ABSTRACT

The ability to precisely manipulate and control extruded materials is essential in the additive manufacturing industry. In addition to the gravity force acting on the extruded medium, here we demonstrate that the employment of a Coulomb force which results from a strategically applied electric field holds a great promise to enhance three-dimensional (3D) printing systems and derive new products. In particular, it is shown experimentally and theoretically that a strategically applied electric field can be used to pre-charge low-volume droplets (non-contact and direct methods), enhancing control during printing. Selectively applying the electric field (E.F.) allows a modified printer more flexibility during a multi-layered print on nearly any chosen substrate. For testing, droplets created on-demand from orifices within inkjet printing parameters were subjected to a transverse electric field. The electric field was generated by retrofitting electrodes to a direct writing (DW)-based 3D printer. The application of electrodes to the print head not only reduced the need for mechanical motion during printing but also revealed novel solutions to problematic printing applications, namely, 3D printing within confinements. These results divulge a plethora of new design opportunities for ink droplet control in 3D printing processes.

1. Introduction

Inkjet-based 3D printing is a widely applied additive manufacturing method that made an industrial-scale transformation from two-dimensional graphical to three-dimensional structural print [1]. It is typically divided into two broad categories determined by the mechanism used to form droplets, continuous inkjet (CIJ) and Drop-on-Demand (DOD) 3D printing. Both techniques produce uniform droplets from the print head. Fueled by a global shift toward lean manufacturing, DOD 3D printing is found to be advantageous over CIJ with less waste and no need for complicated ink recycling systems. DOD 3D printers can form and eject droplets on demand by mechanisms including thermal, piezo, pressure and electrohydrodynamic (EHD) methods. Regardless of the droplet formation methods, it was deemed important that the droplets were produced from a fluid channel within the 10–150 μm diameter range as in the DOD 3D printing literature and industry [2]. For the adaptability of our work in the current DOD 3D printing research and industry, this study herein focuses on investigating droplets with sizes within this range.

Droplet manipulation and resulting metrology are crucial to the advances and applications of DOD-based inkjet 3D printing in many fields, such as bioassays [3–5], chemical and drug delivery [6,7], and electro/mechanical/biological microdevices [8–15]. In these applications, existing manipulation techniques include forming [16,17], transporting [18], merging [19], sorting [17], splitting [20], and storing droplets [21]. Such droplet manipulations can be powered by acoustic waves, electric, magnetic, thermal and hydrodynamic forces and surface tension [22–29]. Among these manipulation techniques, the employment of electric force is one of the most promising methods because of its good compatibility coupled with the short response time. In most cases, the hardware required to create the electric field can be easily integrated into existing machines, making these adaptable technologies highly desirable for today's industry.

Using electric force to manipulate the inkjet 3D printing process holds great promise for specialized applications. The reduction of moving parts, limited impact onto flexible or delicate substrates, and even printing in conventionally hard-to-reach locations (e.g., under an overhang) are just a few of the potential benefits. Doak et al. [30] showed that high-voltage electrodes can be used to deflect a stream of droplets using dielectrophoresis, albeit production and control of an individual droplet was never achieved. In a very recent publication by Liashenko et al. [31], electrostatic jets are deflected using high-voltage electrodes, and when solidified, they create submicrometer features on a translating substrate. Similar to the present work, Liashenko's

electrostatic jet deflection method shows great promise to increase the printing speed and resolution while reducing wear on mechanical stages. However, individual droplet control was not achieved either, which limits the printing geometry accuracy. In addition, as to the authors' knowledge, none of the existing works investigated the feasibility and effectiveness of the electrostatic deflection in drop-on-demand inkjet 3D printing within confinements (e.g., under an overhang).

Against this background, in the present work, we investigated the integration of an electric field in a DOD printing system to manipulate individual droplets through electrostatic charging and deflection. The feasibility of this droplet manipulation method for 3D printing within confinements, which are not accessible by ordinary 3D printing devices, is also explored in the present work. Despite decades of study on the droplet electrostatic charging and deflection, many open questions still exist today [32]. The dispersion and electrical manipulation of droplets are essential to modern engineering [33,34]. Previous efforts of Orme et al. [35–37] extended ink-jet printer applications and deflected metal droplets of small size on an open substrate. However, drop-on-demand 3D printing within confinements, which is the main aim of the present work, has never been attempted. In addition, deflection of non-metal drops demonstrated in the present work involves charging mechanisms different from the metal ones, which deserves exploration. Keeping all this in mind, the present work determined the effective charging mechanism of ink droplets and established the metrology for the electrostatic deflection-assisted 3D printing process. In the rest of the paper, the experimental setup is discussed in section 2. The theoretical analysis is provided in section 3. Results and discussions are presented in section 4, and conclusions are drawn in section 5.

2. Materials and methods

2.1. Experimental setup

To explore ink droplets falling through a transverse electric field, copper electrodes were fitted to a DOD pneumatic print head. The experimental setup consists of a movable x-y table as a support for the collection vessel, two parallel copper electrodes, and a high-voltage power supply, as shown in Fig. 1a. A high voltage is applied to different electrodes via a micro-controller and circuitry.

To generate droplets of diameter d around 1 mm, a commercial droplet generator (Nordson Ultimus I) was used along with a 30-gauge or 32-gauge needle (159 μm and 109 μm inner diameter, respectively). The droplet generator creates a well-defined pressure pulse for a specific time interval driving the ink through a blunt needle at a pressure ranging from 0.1 to 70 psi.

In this study, two distinct droplet-charging techniques were investigated by connecting a selectable charging wire between the grounded electrode and the printing needle. The path for ions in the droplets to be charged or discharged was opened and closed via a high-voltage relay. This relay determined whether the droplets received their charge through direct contact with the printing needle, or through ionized air when falling through the inter-electrode gap (cf. Fig. 1b). The distance between the printing needle and the surface h was kept relatively large as compared to the needle diameter, i.e., $h > 5$ cm, so that droplets have enough time to be positioned between the electrodes during free fall when the electric field was applied. Two vertical electrodes were made of 0.8 cm × 5 cm × 5 cm copper plates adhering to standing dielectric supports made of a 0.7 cm fiberglass board. The distance between the vertical electrodes was fixed at 7.7 cm with the printing needle centered in-between, as illustrated in Fig. 1b and c.

To test the electrostatic deflection and 3D printing process, undiluted glycerol and Spot-E (Spot-A Materials) were used as the materials in the following experiments. Spot-E is a photo-polymerizable resin in the near UV and visible spectrum for applications needing flexibility in typical additive manufacturing processes [38]. It contains 8–25 % aliphatic acrylate, 8–25 % aliphatic urethane crylate, 10–40 %

aromatic acrlylate, 40 % aliphatic acrylate. Its specific gravity is approximately 1.10–1.12, and its apparent viscosity is 100–150 cP at 25 °C according to the data sheet. In the previous work of this group [39], many Direct-Written ink droplets were controlled employing electrowetting. However, this approach did not work with glycerol. Namely, it was impossible to relocated sessile glycerol droplets on horizontal substrates. Motivated by this limitation found in our previous work, glycerol is tested in this study with the aim of proposing an effective electric-field-assisted approach for manipulating deposition of glycerol droplets along the horizontal direction. Spot-E has the kinematic viscosity of $\nu = 3.64 \times 10^{-4}$ m^2/s and was pushed through a 32-gauge needle (108 μm inner diameter) with a syringe pressure of 1.5 psi.

Voltages of 3, 5, 6, 7 and 9 kV applied between the vertical electrodes in the experiments resulted in the electric field strengths of 0.39, 0.65, 0.78, 0.909 and 1.17 kV/cm, respectively (cf. Table 1). The application of 1.17 kV/cm resulted in a droplet deflection at an approximately 45° inclination angle relative to the vertical direction. The electrode voltage was manually controlled with the high-voltage power supply while the polarity was switched by an Arduino micro-controller coupled with a high-voltage relay. These adjustable parameters allow a user-defined control of the droplet motion in the horizontal direction.

The droplet charge was calculated indirectly, by comparing the recorded droplet motion with the theoretical modeling in section 3. This is termed as a primary method of droplet charge measurement. As a secondary method of measuring the droplet charge, a collection vessel was connected to high-impedance buffer and multimeter. The high-impedance buffer is a resistor/capacitor (RC) circuit comprised of 50 k Ω resistor and 100 nF low-leakage capacitor, which were connected to a CA3140 MOSFET operational-amplifier allowing the voltage of the capacitor to be read from the multimeter. By noting the sign of the output voltage, the charge can be identified as either positive or negative.

After initial experiments correlating the droplet charge with its subsequent trajectory when falling through an electric field, the setup was retrofitted to a DIW (Direct Ink Writing) automated dispensing system. Two 0.3 cm × 1.5 cm × 3 cm copper electrodes were attached to a custom dielectric printhead centering the printer's needle within the electric field and located ~8 cm above the substrate, as shown in Fig. 2a. To demonstrate the feasibility of this approach for 3D printing in confinements, a simple overhang structure was prepared for the following test. As shown in Fig. 2, with the developed electrostatic deflection assisted DIW system, droplets were dispensed and selectively deposited on the surface beneath this overhang to build new features.

To safeguard the expensive equipment, the aluminum print bed was replaced with a glass version supported by nylon spacers and bolts. A dielectric printhead was also machined from a Teflon block to insulate the dispensing needle. These were relatively simple precautions and modifications which completely protected the machine and circuitry. The photograph of the modified equipment is shown in Fig. 3. The droplet motion was captured using a high-speed CCD camera (Phantom V210) using back-light shadowgraphy. All experiments were performed under ambient conditions.

3. Theoretical modeling electrostatic charging of droplets

To achieve a desired printing accuracy using the proposed electrostatic-deflection-assisted 3D printing process, the droplet motion and deposition need to be controlled precisely, which requires a method for modeling and measuring the individual droplet charge in the process. It is known that the charge relaxation times τ_C of liquids range from 1 μs to 20 s [40]. Glycerol, in particular, has the charge relaxation time on the order of 3 μs. The characteristic hydrodynamic time τ_H, which is the residence time of liquid volume in the needle, is ~0.43 s in this study. Because $\tau_C << \tau_H$, glycerol behaves in the present experiments as a perfect conductor and droplets can become charged in
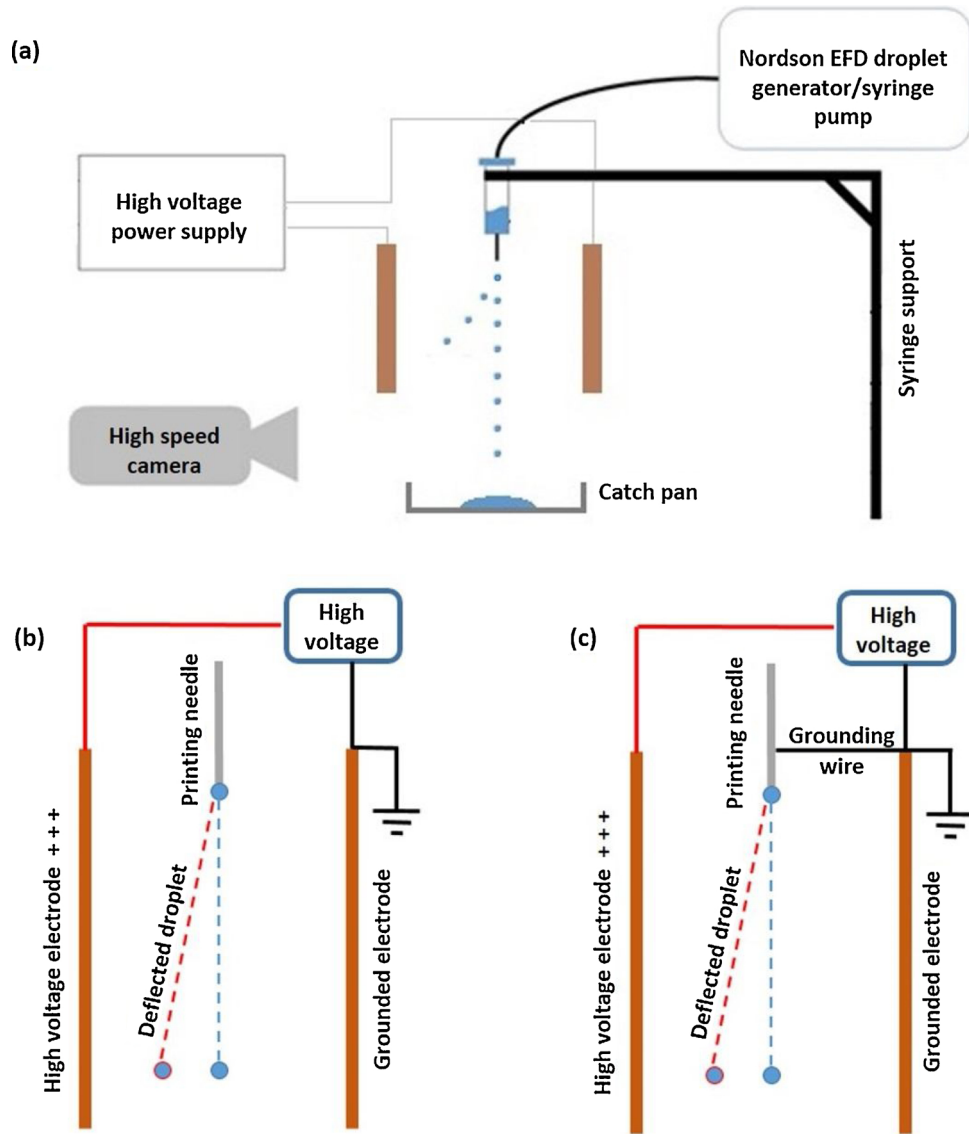
Fig. 1. (a) Schematic of the experiment setup. (b) Electrode design without a grounded needle. (c) Electrode design with a grounded needle.

Table 1
Correlation between voltage and E.F. strength.

Voltage (kV)	E.F. Strength (kV/cm)
3	0.39
5	0.65
6	0.78
7	0.91
9	1.17

the needle [41].

Charged pendant droplets at the needle's exit are subjected to both gravity and Coulomb forces resulting from the electric field imposed by the electrodes. These forces detach the droplet from the needle. Then, free fall determined by gravity and Coulomb forces begins. Droplet motion in the free fall is described by the second law of Newton, which takes the following form:

$$m\frac{d^2\mathbf{r}}{dt^2} = -mg\mathbf{k} + QE\mathbf{i} \tag{1}$$

where t is time, m is the droplet mass, $\mathbf{r}$ is its radius-vector, g is the magnitude of gravity acceleration, $\mathbf{i}$ and $\mathbf{k}$ are unit vectors of the horizontal and vertical directions, respectively, Q is the droplet charge, and E is the electric field strength imposed by the electrodes.

Projections of Eq. (1) on the horizontal and vertical axes yield:

$$m\frac{d^2x}{dt^2} = QE, \quad \frac{d^2z}{dt^2} = -g \tag{2}$$

The droplet detachment moment is taken as $t = 0$, and Cartesian coordinates at the needle exit are set as $x = 0$ and $z = h$. Accordingly, the following initial conditions are imposed on the solutions of Eq. (2)

$$at\ t = 0, \quad x = 0, \ z = h, \ \frac{dx}{dt} = \frac{dz}{dt} = 0 \tag{3}$$

Solutions of Eq. (2) subjected to the initial conditions (3) read:

$$x = \frac{QE}{m}\frac{t^2}{2}, \quad z = -g\frac{t^2}{2} + h \tag{4}$$

The substrate on which droplets impact is located at plane $z = 0$. Then, the impact moment is $t_* = \sqrt{2h/g}$ and the horizontal coordinate of the impact location is

$$x_* = \frac{QEh}{mg} \tag{5}$$

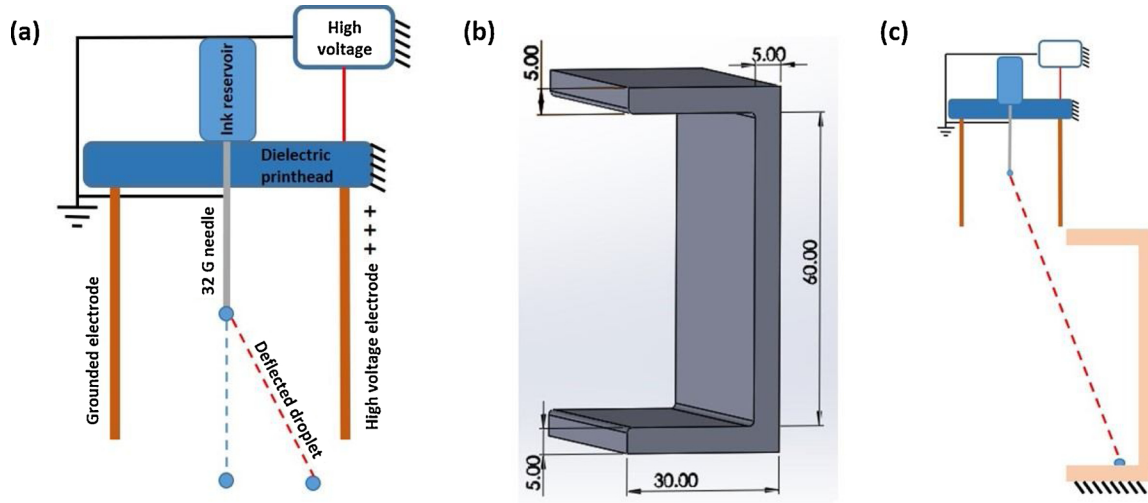Moreover, Eq. (4) yields the droplet trajectory in flight as a straight

Fig. 2. (a) Schematic of the print head retrofitted with electrodes. (b) A CAD drawing of overhang structure (a model confinement) with all dimensions (mm). (c) The trajectory of ink droplets as a modified printhead overcomes the problematic printing situation caused by an overhang structure.

line described by:

$$x = \frac{QE}{m}\frac{(h-z)}{g} \tag{6}$$

In addition, Eq. (5) expresses the droplet charge, still unknown, as

$$Q = \frac{mgx_*}{Eh} = \frac{mgx_*L}{Vh} \tag{7}$$

where V is the applied voltage, and L is the distance between electrodes.

Droplet mass was measured using its images and the known density under the assumption that the droplet is spherical. The landing position x_* was measured using the video images. Accordingly, the second Eq. (7) can be employed to measure the droplet charge Q. A calculated volumetric flow rate $\dot{Q}$ is used for comparisons and found using Eq. (8)

$$\dot{Q} = \frac{pR^2}{8\mu l} \tag{8}$$

Here p is the applied pressure to the syringe, R is the inner radius of the needle, μ is the dynamic viscosity of the ink, and l is the length the needle through which the ink must be pushed.

4. Results and discussion

4.1. Charging mechanism

In this study, two approaches to droplet charging were investigated. In the first case, the printing needle was directly connected to the grounded electrode, as shown in Fig. 1c. This configuration provides a direct path for ion exchange, ultimately leading to glycerol polarization (charging). On the other hand, in the second approach, the printing
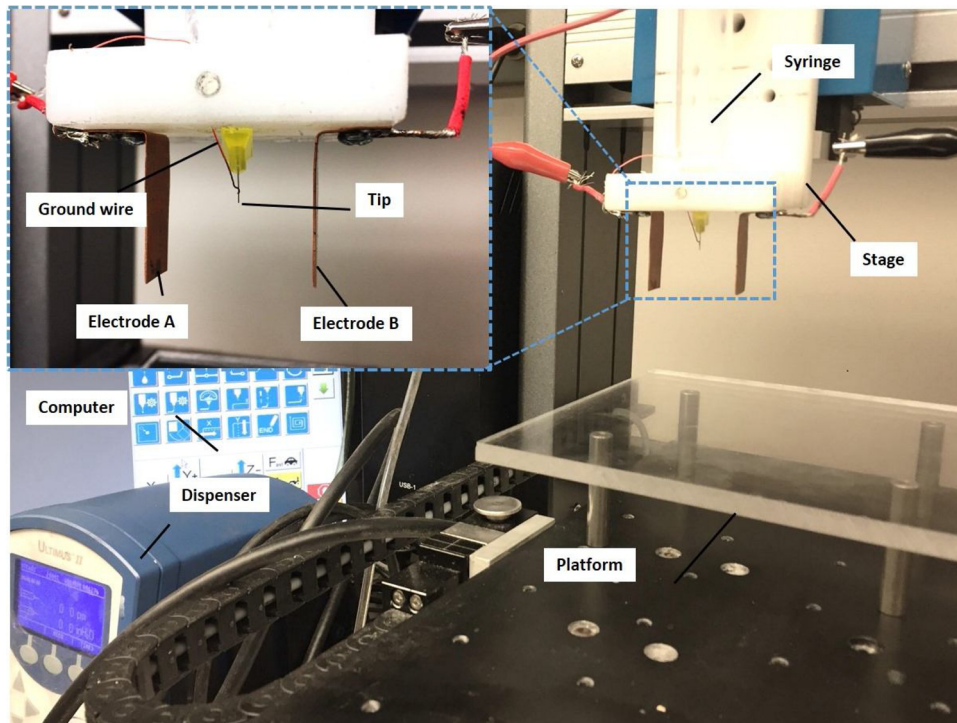

Fig. 3. Photo of a retrofitted DIW (Direct Ink Writing) system setup utilizing DOD generation within a transverse electric field.
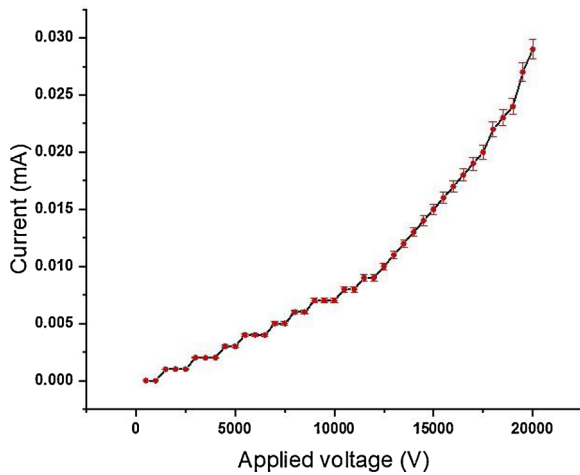
Fig. 4. Measured current/voltage characteristics of the inter-electrode gap. The experimental data is shown by symbols spanned by a line.

needle was disconnected from the grounded electrode, with the droplet charging solely relying on the charge transferred from the ionized air within the inter-electrode gap during the droplet fall, as shown in Fig. 1b. Fig. 4 reveals the measured electric current-voltage characteristic of the inter-electrode gap determined by air ionization by the transverse electric field. To track the droplet motion, high-speed videos of droplets in flight were recorded. These droplets and the corresponding trajectories were analyzed frame by frame by an in-house Matlab program.

4.2. Droplet geometry evolution

In this section, the study of droplet geometry evolution was explored to understand the in-flight behavior. As recorded by the high-speed videos, immediately after detachment from the needle, a tear-like droplet shape is observed, as demonstrated in Fig. 5. As time progresses, surface tension rounds the droplet off (Fig. 5c and d). Such images are convenient for further analysis, and they were taken in the height range marked by the two horizontal dashed-dotted lines in Fig. 5c. It is important to note that Fig. 5b and d show larger droplets formed to accentuate the shapes and features of the falling droplets during review and initial experiments. It should also be noted that all other droplets produced and studied are below the 1 mm diameter and larger than the 150 μm capillary to meet the inkjet requirements, unless otherwise stated. Still, slight oscillations of the droplets are evident with the oblate and prolate spheroidal shapes observed throughout the entire fall.

To understand the influence of the electric field on the droplet size, two methods of droplet charging described in section 2 using the voltage of 3 − 6 kV. It was found that with both air ionization and direct charging of a droplet by a wire electrode, the size of the falling droplet is inversely proportional to the applied voltage. Fig. 6 shows a series of detaching droplet snapshots taken in the initial experiments utilizing larger droplets for clarity. The snapshots clearly show a dramatic effect on the diameter of droplets of the increasing applied voltage.

As the voltage is increased throughout the series of pictures shown in Fig. 6, the resulting Coulomb force combines with the gravitation force already acting on the body of the droplet. If the E.F. strength becomes too high however, the pull on the pendant droplet will become strong enough to stretch the fluid to the electrode in a similar manner to EHD (electrohydrodynamic) printing. Another possible cause of the reduced droplet size might be related to the shear force introduced by the E.F. which might stretch the solid/liquid contact area in an undesirable way when compared to pure tension between the needle and the droplet.

Under the electric field, since the flow rate through the printing

needle is independent of the applied voltage, a reduction in the droplet size is required to compensate for the periodic detachment of droplets. Fig. 7 illustrates the measured relationship between the droplet mass, the detachment frequency and the imposed volumetric flow rate. The difference between the measured and calculated flow is likely due to errors in the needle radius, viscosity and pressure-reading errors.

4.3. Droplet charging

The average charges on droplets established via Eq. (7) and the experimental data for the landing location for both charging methods at several values of the applied voltage are presented in Fig. 8.

It was established in Fig. 7a that as the electric field strength between the electrodes increases, the mass of the droplets m can decrease. Then, using the data from Fig. 7a, one can determine the specific droplet charge $q = Q/m$, which is presented in Fig. 9. It is seen that the specific charge strongly increases with the applied voltage for both methods of charging. It should be noted that since the error in Fig. 9 is the ratio of two variables, Taylor expansion was used to estimate(< 10 %) $Var(r) = Var(X/Y)$, where r, x, and y are the means of their distributions, calculated by Eq. (9) and depicted by the error bars in Fig. 9

$$Var(r) = r^2 \left[\frac{Var(y)}{y^2} + \frac{Var(x)}{x^2} - \frac{2Cov(x, y)}{xy} \right] \tag{9}$$

In addition, Fig. 10 shows that the charge per unit surface area q_a, on the droplet, also increases with the applied voltage.

An independent, direct measurement of droplet charge Q was done using the equation for capacitance of a parallel-plate capacitor. 100 droplets were dripped into a conductive collector which was insulated from its surroundings. The cumulative charge of these droplets was transferred to a capacitor of a known capacitance, where with the help of a buffering op-amp, the voltage was recorded using a multimeter. The specific charge found by this independent method is then compared to the one found via Eq. (7), which reveals a reasonably accurate agreement. It should be noted that the droplet's charge due to solely air ionization was too small to be measured with the buffered capacitor setup, and therefore, the direct droplet charging with the grounded wire attached to the needle is preferable.

Transferring a charge to the ink droplet has enabled one in positioning the ejected droplets within an electric field following detachment from the needle. Accordingly, the experimental setup can be reduced in size allowing attachment to a commercial DIW printer. DIW printers operate very close to the printing surface, and thus are set to a home position calibrating the standoff distance (distance from print needle to substrate) before printing can commence. By eliminating this calibration (homing) on the z-stage and limiting the printing needle to a specific plane ∼ 8 cm above the substrate, the commercial DIW printer effectively transformed into a DOD inkjet printer prototype previously described by the schematic in Fig. 2. Here, adding electrodes along with a high-voltage power supply and required circuitry allowed additional control of the droplets after ejection. Two liquids were chosen for testing on the modified printer. To keep in line with the previous experiment, glycerol was the first fluid tested, while a photo-resin polymer ink (Spot-E, Spot-A Materials) was also chosen to explore operation with commercially available industrial materials. It should be emphasized that for all the following printing scenarios, the print head was fixed the z-direction. The print head moved only along the y-axis while the droplets were positioned along the x-axis by means of the electric field which acted on the droplets falling vertically (against the z-axis).

4.4. Trajectories

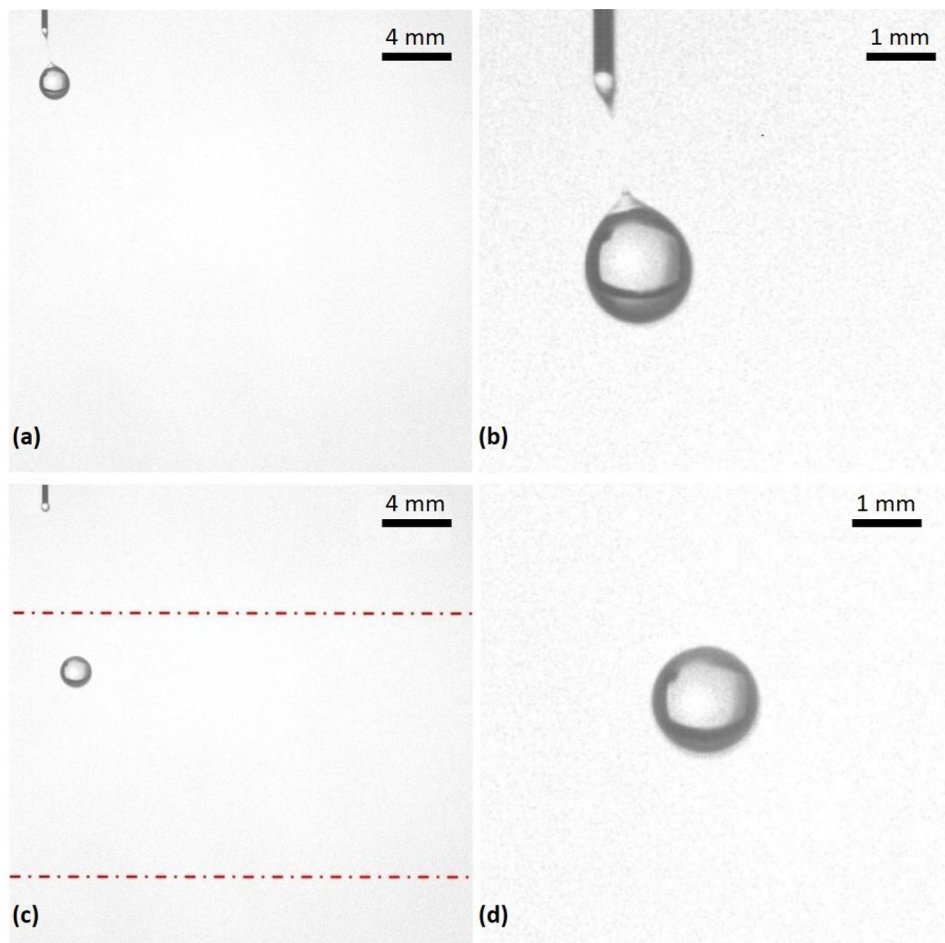The recorded droplet trajectories were established frame by frame

Fig. 5. (a) Global view of tear-like droplet just detached from the printing needle. (b) Magnified image of tear-like droplet just detached from the printing needle. (c) Spherical droplet in the range used for further analysis (the area between the two red dashed lines). (d) Magnified image of spherical droplet in the range used for further analysis. Note that large droplets (b) and (d) were photographed to visually capture tear-like tail and spherical droplet.

using video recordings for hundreds of droplets. The measured droplet trajectories appeared to be linear in agreement with the predictions of Eq. (6); cf. Fig. 11. Superimposing the predicted trajectory (6) with the experimental data allows one to find the droplet charge Q, using the measured droplet mass m. Also, this can be done directly using Eq. (7) and the measured horizontal droplet landing coordinate x_*.

On the other hand, Fig. 12 compares the effect of the droplet charging method on their trajectories. The larger horizontal droplet deflections reveal that the direct charging by the wire electrode allows for a higher droplet charge than the one acquired from the ionized air in the case of indirect charging at the same voltage (5–7 kV). Note that at

3 kV, droplet charging by ionized air resulted in a practically un-noticeable horizontal deflection, and this data is not included in Fig. 12.

4.5. Test cases

Initial tests on the retrofitted DIW printer used glycerol as the working fluid with the 30-gauge printing needle fixed about 6.5 cm above the glass substrate supported by the print bed. While the 30-gauge needle is slightly larger (159 μm) than the $10-150$ μm range found in inkjet literature, the size was selected to simplify the initial case and maximize viewing potential. The pressure was set to 5 psi.
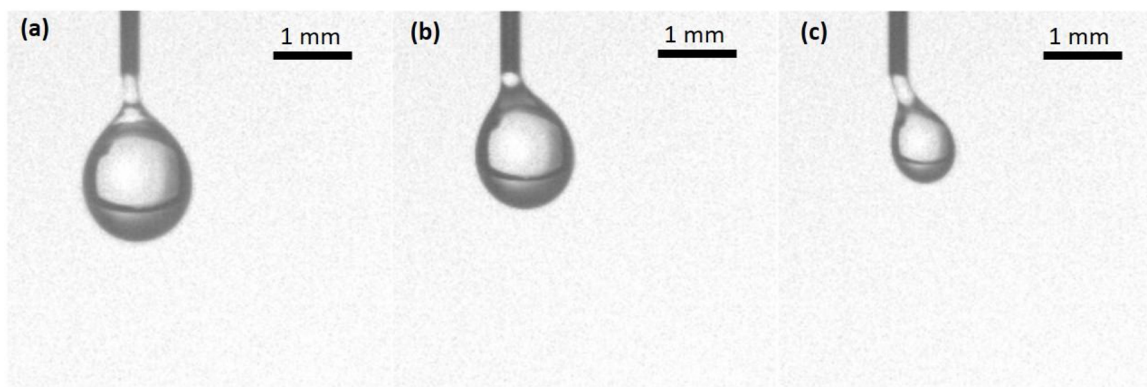

Fig. 6. Detaching droplets at the following applied voltages: (a) 3 kV, (b) 5 kV, (c) 6 kV. The printing needle is grounded in all cases.

(a)
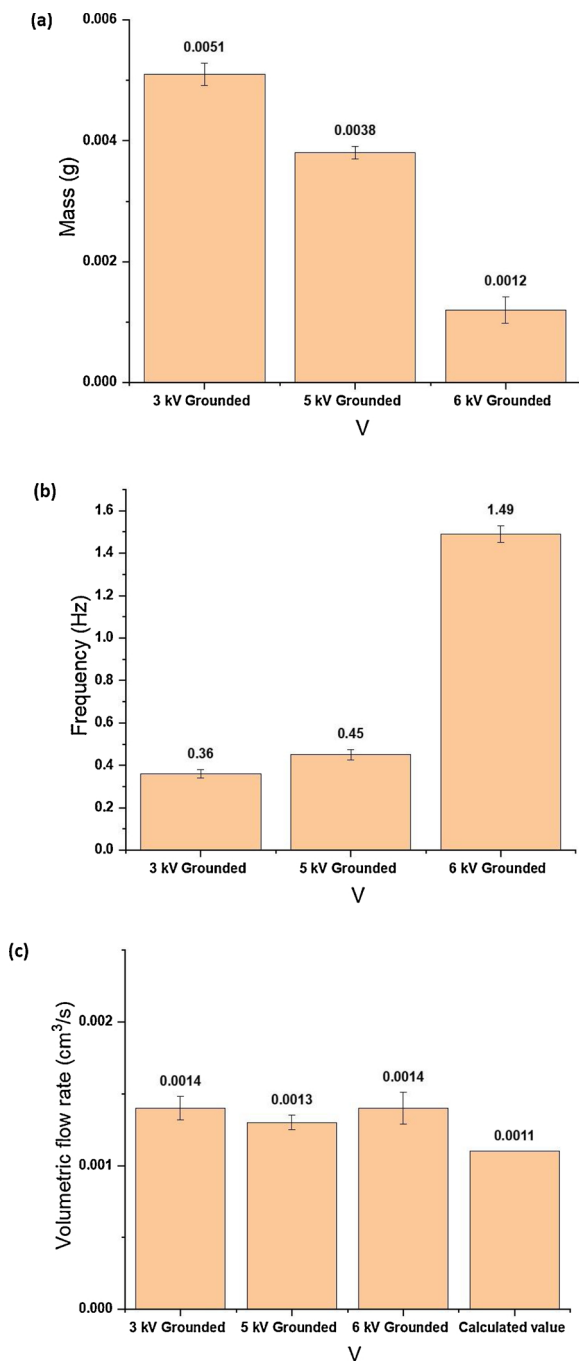

(b)

(c)

Fig. 7. Droplet mass (a), detachment frequency (b), and the imposed volumetric flow rate along with calculated flow using Eq. (8). (c) at three different values of the applied voltage (3, 5 and 6 kV) in the case of grounded printing needle.

Fig. 13a shows the expected placements of glycerol droplets numbered sequentially in their order of printing for each y-position (cf. Table 2). The capital letters set to subscript each droplet represent specific electric filed strengths (cf. Table 3). It should be emphasized that the absence of subscript denotes the no-electric-field-applied cases. Fig. 13b shows a photo of the corresponding glycerol print.

Table 2 details the y-positions during glycerol printing along with the number of droplets ejected to each location. Table 3 details the voltages and the corresponding electric field strengths of each high-voltage setting used to move the droplets along the x-axis. Parameters of each printed droplet can be found in the schematic in Fig. 13a combined with the associated Tables 2 and 3 [e.g., the first leg of the U
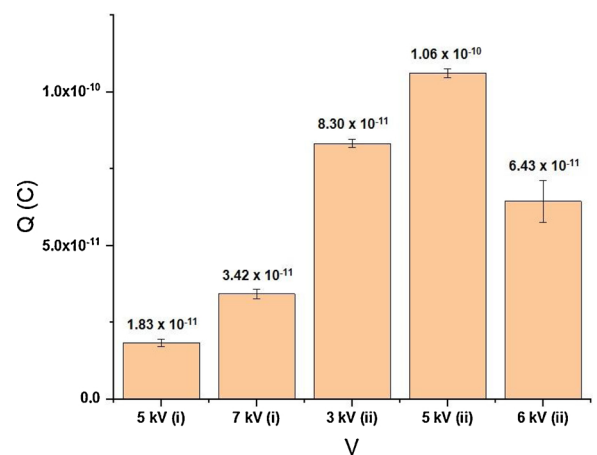

Fig. 8. The average charge of glycerol droplets found using Eq. (7) and the experimentally measured droplet landing location. Charging by ionized air is denoted as (i), whereas direct charging by wire electrode as (ii).
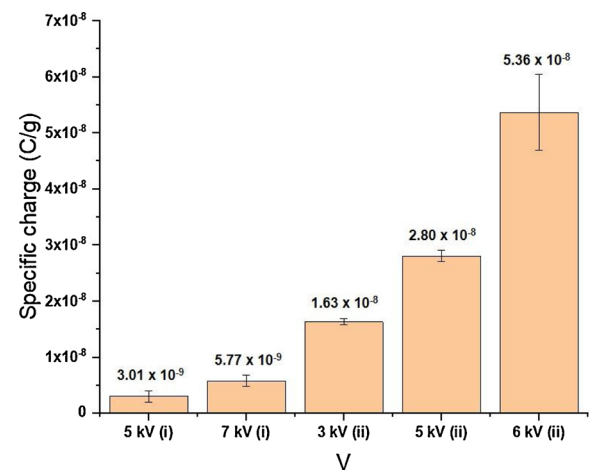

Fig. 9. The specific charge of glycerol droplets. Charging by ionized air is denoted as (i), whereas direct charging by wire electrode as (ii).
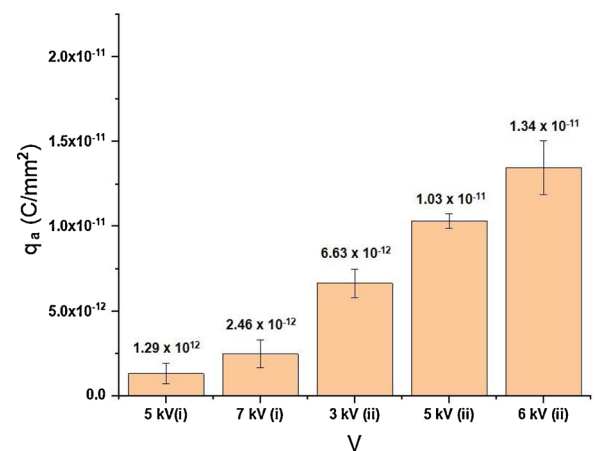

Fig. 10. Charge per unit surface area on glycerol droplets. Charging by ionized air is denoted as (i), whereas direct charging by wire electrode as (ii).

letter in UIC was printed at position y_1 (0,0), where 5 droplets were deposited]. The first droplet was placed with no voltage applied, the second one was placed with 2.3 kV, while the third droplet was placed with 2.4 kV, etc.

After the initial test with glycerol on the prototype printer retro-fitted with high-voltage electrodes, the working fluid was changed to
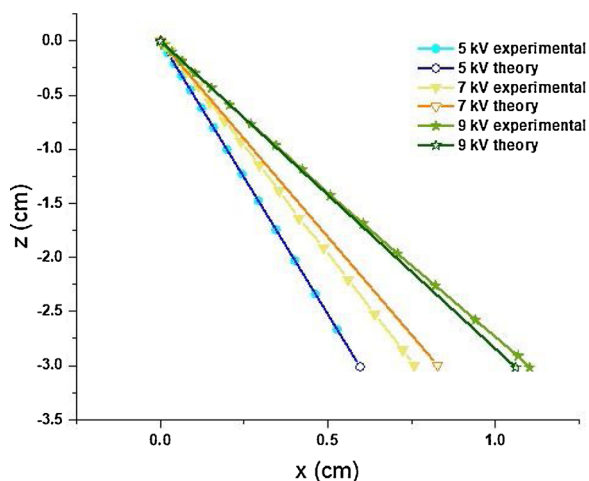
Fig. 11. Droplet trajectories in the case of charging by ionized air as in Fig. 1b. Experimental data are shown by symbols, the trajectories predicted by Eq. (6)- by straight lines with open symbols corresponding to the listed applied voltages.
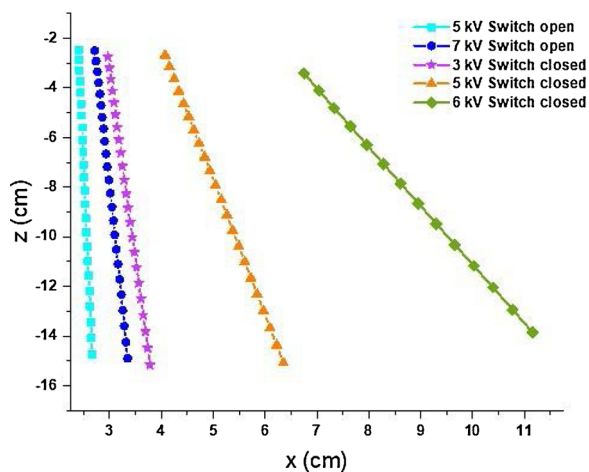

Fig. 12. Droplet trajectories resulting from the two different methods of droplet charging denoted in the panel.

Spot-E photo-resin. The printing needle was also changed to a 32-gauge needle, which at 108 µm, falls within the inkjet range from the literature. The pressure was reduced to 1.5 psi. Fig. 14a shows the expected placements of Spot-E droplets numbered sequentially in their order of printing for each y-position. The ability to cure the photo-resin with UV light allowed multiple layers of the ink to be printed. The UV light used in this study was an uvBeast (uvBeast UVB-01 V3 365 nm UV Flashlight, 5400 µW/cm^2). The UV light was set up to directly project light to the printing substrate. For one single droplet, the curing time is smaller than 3 s. In multilayer printing, droplets for the second layer were jetted after the first layer is solidified. The first layer of deposited ink measured 0.44 mm thick, while the addition of the second layer resulted in a thickness of 0.67 mm. Fig. 14b shows a photo of the dual-layer Spot-E print.

Table 4 lists the y-positions during the dual-layer Spot-E printing along with the number of droplets ejected at each location.

Table 5 lists the voltages and the corresponding electric field strengths of each high-voltage setting used to move the droplets along the x-axis.

To demonstrate novel capabilities of the proposed method, 3D printing inside a confinement (an overhang) in Fig. 2b is explored next. This would be a problematic printing situation for any ordinary 3D printing device, but not for the present electrically-assisted one, as is
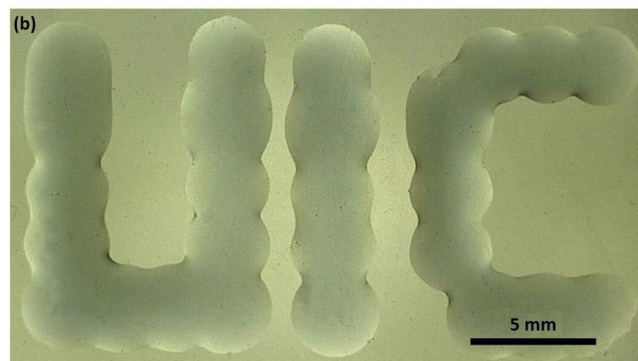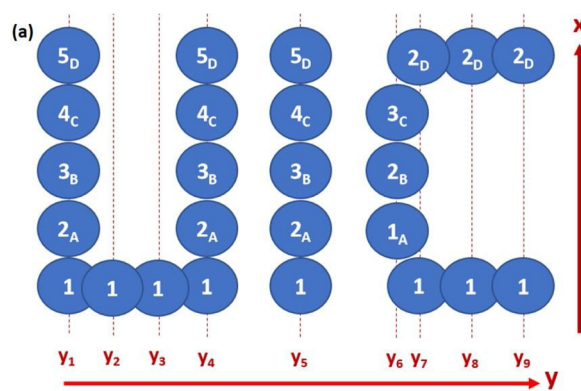

Fig. 13. (a) Schematic of intended glycerol droplet locations. (b) Photo of printed glycerol on a glass substrate.

Table 2

Listing of the y-positions during printing and the number of droplets ejected at each position.

Position	y (mm)	Number of Droplets
y_1	0.0	5
y_2	2.5	1
y_3	5.0	1
y_4	7.5	5
y_5	12.0	5
y_6	16.5	3
y_7	18.0	2
y_8	20.5	2
y_9	23.0	2

Table 3

Listing of voltage and the corresponding E.F. strength during printing.

High-Voltage Setting	Voltage (kV)	EF Strength (kV/cm)
A	1.35	0.45
B	1.80	0.60
C	2.15	0.72
D	2.45	0.82

depicted in Fig. 2c. Moreover, this particular situation is not just problematic for DIW and inkjet printers but to all known sub-classes of conventional or 3D printing processes researched until now, as to our knowledge.

The 32 G printing needle was employed with the pressure remaining at 1.5 psi. Fig. 15a shows the expected placements of Spot-E droplets numbered sequentially in their order of printing for each y-position. It should be emphasized that every droplet should be affected by the electric field in this case, as every droplet must be deflected from vertical to ultimately land beneath the overhang (inside the confinement).
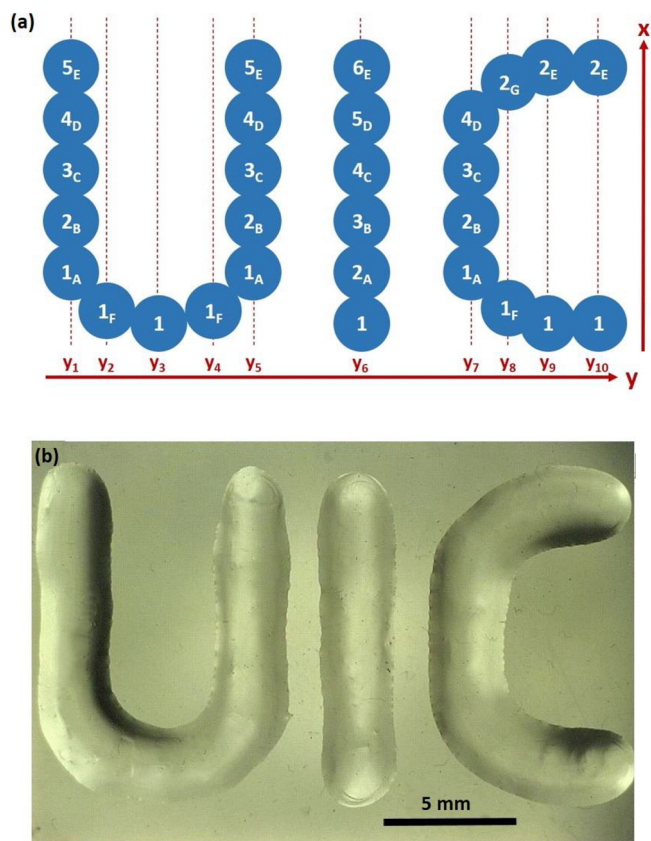
Fig. 14. (a) Schematic of intended Spot-E droplet locations numbered sequentially in printing order. This procedure was repeated twice to achieve a dual-layer print. (b) Photo of dual-layer Spot-E print.
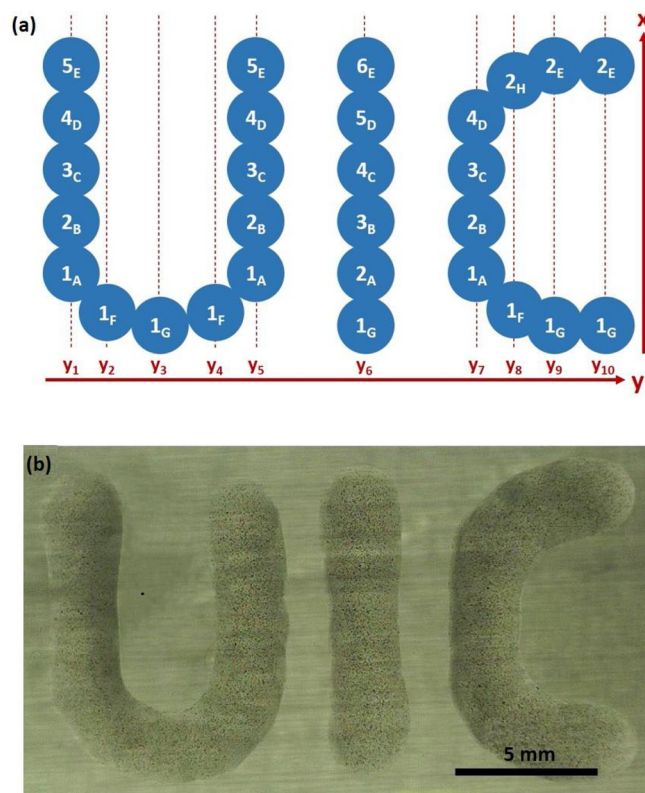

Fig. 15. (a) Schematic of intended Spot-E droplet locations to be printed below the problematic overhang structure (inside a confinement) and numbered sequentially in printing order. Lettered subscripts denote specific applied voltages corresponding to different electric field strengths. (b) Backlit photo (taken orthogonal to the x-axis) of Spot-E printed below problematic overhang structure comprised of VeroClear RGD-810 photo-resin.

Table 4

Listing of the y-positions during dual-layer Spot-E printing along with the number of droplets ejected at each position.

Position	y (mm)	Number of Droplets
y_1	0.0	5
y_2	1.5	1
y_3	3.5	1
y_4	5.5	1
y_5	7.0	5
y_6	1.0	6
y_7	15.0	4
y_8	16.5	2
y_9	18.5	2
y_{10}	21.5	2

Table 5

Listing of voltage and the E.F. strength during dual-layer Spot-E printing.

High-Voltage Setting	Voltage (kV)	EF Strength (kV/cm)
A	1.35	0.45
B	1.75	0.58
C	2.15	0.72
D	2.30	0.77
E	2.50	0.83
F	1.20	0.40
G	2.45	0.82

Table 6

Listing of the y-positions used while printing beneath the problematic overhang structure along with the number of droplets issued.

Position	y (mm)	Number of Droplets
y_1	0.0	5
y_2	1.5	1
y_3	3.5	1
y_4	5.5	1
y_5	7.0	5
y_6	11.0	6
y_7	15.0	4
y_8	16.5	2
y_9	18.5	2
y_{10}	21.5	2

Table 7

Listing of voltage and the E.F. strength while printing beneath the overhang.

High-Voltage Setting	Voltage (kV)	E.F. strength (kV/cm)
A	2.45	0.82
B	2.55	0.85
C	2.65	0.88
D	2.72	0.91
E	2.82	0.94
F	2.34	0.78
G	2.30	0.77
H	2.78	0.93

Fig. 15b shows a photo of the UIC logo printed beneath the printed overhang structure.

Table 6 details the y-positions used while printing beneath the problematic overhang structure.

Table 7 details the voltages and the corresponding electric field strengths of each high-voltage setting used to move the droplets along the x-axis and below the overhang.

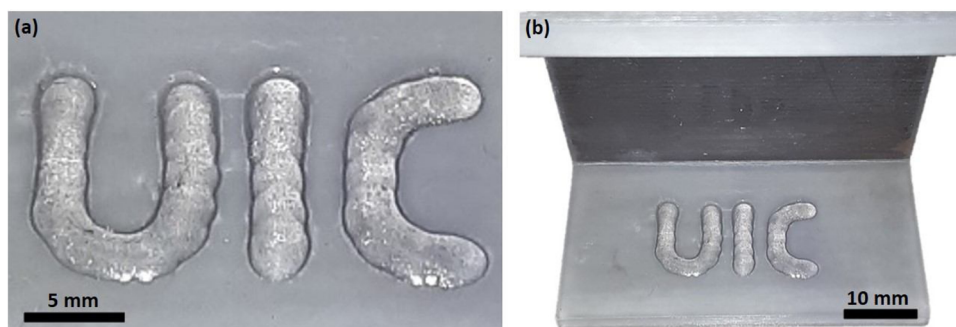An alternative view, taken at about 45° is depicted in both Fig. 16a

Fig. 16. (a) Photo (taken at about 45° from horizontal) of Spot-E printed below the problematic overhang structure (in confinement). (b) A zoomed-out photo revealing the overhang structure with a printed logo inside.

and b shown at two different magnifications.

5. Conclusion

The present experimental and theoretical results reveal that an electric field, strategically generated near a printing orifice, can be used to selectively place ink droplets. By evaluating the droplet charge using joint theoretical and experimental efforts, an accurate and repeatable movement of droplets was achieved by means of the Coulomb force imposed by the transverse electric field. In previous works of the present group, it was found that glycerol was incapable of movement on the surface by means of electrowetting-on-dielectrics in 3D printing applications. However, in the present work, it was demonstrated that glycerol droplets can be positioned by the applied electrostatic force during droplet flight. Next, a commercially available printer was modified by inclusion of the transverse electric field and used to print a photo-initiative ink Spot-E. Specifically, a straightforward addition of two electrodes to the printhead, was able to reduce moving parts, deposit droplets onto flexible substrates without splashing, and even print in conventionally hard-to-reach locations, such as under an overhang confinement. In a sense, one of the methods proposed in this work pulls closer the domains of 3D printing, electrospinning and electrospraying [42]. The present innovative approach holds great promise for (i) generation techniques aimed at reduced droplet volumes for greater resolution, and (ii) 2D droplet control by addition of a second set of electrodes oriented by 90° about the y-axis.

CRediT authorship contribution statement

J. Plog: Writing - original draft, Conceptualization, Methodology, Visualization, Investigation, Theory. **Y. Jiang:** Data curation, Methodology, Investigation. **Y. Pan:** Supervision, Validation, Writing - review & editing. **A.L. Yarin:** Supervision, Theory, Validation, Writing - review & editing.

Declaration of Competing Interest

The authors declare that they have no known competing financial interests or personal relationships that could have appeared to influence the work reported in this paper.

Acknowledgment

Appendix A. Supplementary data

Supplementary material related to this article can be found, in the online version, at doi:https://doi.org/10.1016/j.addma.2020.101400.

References

[1] A. Sridhar, T. Blaudeck, R. Baumann, Inkjet printing as a key enabling technology for printed electronics, Mater. Matters 6 (2011) 12–15.

[2] B. Derby, Inkjet printing of functional and structural materials: fluid property requirements, feature stability, and resolution, Annu. Rev. Mater. Res. 40 (2010) 395–414.

[3] B. Hadwen, G.R. Broder, D. Morganti, A. Jacobs, C. Brown, J.R. Hector, Y. Kubota, H. Morgan, Programmable large area digital microfluidic array with integrated droplet sensing for bioassays, Lab Chip 12 (2012) 3305–3313.

[4] O. Loh, R. Lam, M. Chen, N. Moldovan, H. Huang, D. Ho, H.D. Espinosa, Nanofountain-probe-based high-resolution patterning and single-cell injection of functionalized nanodiamonds, Small 5 (2009) 1667–1674.

[5] R.U. Meckenstock, F. Netzer, C. Stumpp, T. Lueders, A.M. Himmelberg, N. Hertkorn, P. Schmitt-Kopplin, M. Harir, R. Hosein, S. Haque, D. Schulze, Water droplets in oil are microhabitats for microbial life, Science 345 (2014) 673–676.

[6] A. René, C. Cugnet, D. Hauchard, L. Authier, Elaboration of screen-printed microelectrodes working as generator/collector and their use in a flow cell system, Sens. Actuators B Chem. 174 (2012) 225–230.

[7] B.E. Rabinow, Nanosuspensions in drug delivery, Nat. Rev. Drug Discov. 3 (2004) 785–796.

[8] A. Bietsch, J. Zhang, M. Hegner, H.P. Lang, C. Gerber, Rapid functionalization of cantilever array sensors by inkjet printing, Nanotechnology 15 (2004) 873–880.

[9] Y. Zhang, J. Stringer, R. Grainger, P.J. Smith, A. Hodzic, Fabrication of patterned thermoplastic microphases between composite plies by inkjet printing, J. Compos. Mater. 49 (2015) 1907–1913.

[10] T. Unander, H. Nilsson, Characterization of printed moisture sensors in packaging surveillance applications, IEEE Sens. J. 9 (2009) 922–928.

[11] H. Sirringhaus, T. Kawase, R.H. Friend, T. Shimoda, M. Inbasekaran, W. Wu, E.P. Woo, High-resolution inkjet printing of all-polymer transistor circuits, Science 290 (2000) 2123–2126.

[12] C. Choi, L. Lin, C. Cheng, C. Chang, Printed oxide thin-film transistors: a mini-review, ECS J. Solid State Sci. Technol. 4 (2015) 3044–3051.

[13] C.J. Ferris, K.J. Gilmore, S. Beirne, D. McCallum, G.G. Wallace, Bio-ink for on-demand printing of living cells, Biomater. Sci. 1 (2013) 224–230.

[14] K. Zhang, C. Chou, X. Xia, M. Hung, L. Qin, Block-Cell-Printing for live single-cell printing, Proc. Natl. Acad. Sci. U. S. A. 111 (2014) 2948–2953.

[15] P. Calvert, Printing cells, Science 318 (2007) 208–209.

[16] S.L. Anna, N. Bontoux, H.A. Stone, Formation of dispersions using "flow focusing" in microchannels, Appl. Phys. Lett. 82 (2003) 364–366.

[17] L.M. Fidalgo, G. Whyte, D. Bratton, C.F. Kaminski, C. Abell, W.T. Huck, From microdroplets to microfluidics: selective emulsion separation in microfluidic devices, Angew. Chem. Int. Ed. 47 (2008) 2042–2045.

[18] S.K. Cho, H. Moon, C. Kim, Creating, transporting, cutting, and merging liquid droplets by electrowetting-based actuation for digital microfluidic circuits, J. Microelectromech. Syst. 12 (2003) 70–80.

[19] L.H. Hung, K.M. Choi, W.Y. Tseng, Y.C. Tan, K. Shea, A.P. Lee, Alternating droplet generation and controlled dynamic droplet fusion in microfluidic device for CdS nanoparticle synthesis, Lab Chip 6 (2006) 174–178.

[20] D. Link, S.L. Anna, D.A. Weitz, H. Stone, Geometrically mediated breakup of drops in microfluidic devices, Phys. Rev. Lett. 92 (2004) 54503.

[21] W. Wang, C. Yang, C.M. Li, On-demand microfluidic droplet trapping and fusion for on-chip static droplet assays, Lab Chip 9 (2009) 1504–1506.

[22] X. Niu, S. Gulati, J.B. Edel, A. deMello, Pillar-induced droplet merging in microfluidic circuits, Lab Chip 8 (2008) 1837–1841.

[23] T. Franke, A.R. Abate, D.A. Weitz, A. Wixforth, Surface acoustic wave (SAW) directed droplet flow in microfluidics for PDMS devices, Lab Chip 9 (2009) 2625–2627.

[24] L. Zhao, L. Pan, K. Zhang, S. Guo, W. Liu, Y. Wang, Y. Chen, X. Zhao, H. Chan, Generation of Janus alginate hydrogel particles with magnetic anisotropy for cell encapsulation, Lab Chip 9 (2009) 2981–2986.

[25] N.T. Nguyen, T.H. Ting, Y.F. Yap, T.N. Wong, J. Chai, W. Ong, J. Zhou, S. Tan, L. Yobas, Thermally mediated droplet formation in microchannels, Appl. Phys. Lett. 91 (2007) 084102–084103.

[26] S. Tan, S. Murshed, N. Nguyen, T. Wong, L. Yobas, Thermally controlled droplet

formation in flow-focusing geometry: formation regimes and effect of nanoparticle suspension, J. Phys. D Appl. Phys. 41 (2008) 165501.

[27] M. He, J. Edgar, G.D.M. Jeffries, R. Lorenz, J. Shelby, D.T. Chiu, Selective encapsulation of single cells and subcellular organelles into picoliter- and femtoliter-volume droplets, Anal. Chem. 77 (2005) 1539–1544.

[28] M. Ozkan, M. Wang, C. Ozkan, R. Flynn, S. Esener, Optical manipulation of objects and biological cells in microfluidic devices, Biomed. Microdevices 5 (2003) 61–67.

[29] S. Zeng, B. Li, X. Su, J. Qin, B. Lin, Microvalve-actuated precise control of individual droplets in microfluidic devices, Lab Chip 9 (2009) 1340–1343.

[30] W. Doak, J. Donovan, P. Chiarot, Deflection of continuous droplet streams using high-voltage dielectrophoresis, Exp. Fluids 54 (2013) 1577.

[31] I. Liashenko, J. Rosell-Llompart, A. Cabot, Ultrafast 3D printing with sub-micrometer features using electrostatic jet deflection, Nat. Commun 11 (2020) 753.

[32] G. Martin, S. Hoath, I. Hutchings, Inkjet printing - the physics of manipulating liquid jets and droplets, J. Phys. Conf. Ser. 105 (2008) 012001.

[33] L. Zhang, H. Liu, Y. Zhao, X. Sun, Y. Wen, Y. Guo, X. Gao, C.-a. Di, G. Yu, Y. Liu, Inkjet printing high-resolution, large-area graphene patterns by coffee-ring lithography, Adv. Mater. 24 (2012) 436–440.

[34] M. Singh, H.M. Haverinen, P. Dhagat, G.E. Jabbour, Inkjet printing-process and its applications, Adv. Mater. 22 (2010) 673–685.

[35] Q. Liu, M. Orme, High precision solder droplet printing technology and the state-of-the-art, J. Mater. Process. Technol. 115 (2001) 271–283.

[36] M. Orme, A novel technique of rapid solidification net-form material synthesis, J. Mater. Eng. Perform. 2 (1993) 399–405.

[37] M. Orme, C. Huang, J. Courter, Precision droplet-based manufacturing and material synthesis: fluid dynamics and thermal control issues, Atomization Sprays 6 (1996) 305–329.

[38] L. Lu, Z. Zhang, J. Xu, Y. Pan, 3D-printed polymer composites with acoustically assembled multidimensional filler networks for accelerated heat dissipation, Compos. Part B Eng. 174 (2019) 106991.

[39] J. Plog, J. Löwe, Y. Jiang, Y. Pan, A.L. Yarin, Control of direct written ink droplets using electrowetting, Langmuir 35 (2019) 11023–11036.

[40] S.A. Theron, E. Zussman, Electric and magnetic parameters of liquids and gases, in: C. Tropea, A.L. Yarin, J. Foss (Eds.), Springer Handbook of Experimental Fluid Mechanics, Springer, Berlin, 2007 Chapter 3.7.

[41] S.N. Reznik, A.L. Yarin, E. Zussman, L. Bercovici, Evolution of a compound droplet attached to a core-shell nozzle under the action of a strong electric field, Phys. Fluids 18 (2006) 062101.

[42] A.L. Yarin, B. Pourdeyhimi, S. Ramakrishna, Fundamentals and Applications of Micro- and Nanofibers, Cambridge University Press, Cambridge, 2014.